

Characterizing $S = 3/2$ AKLT Hamiltonian with Scanning Tunneling Spectroscopy

M. Ferri-Cortés¹, J. C. G. Henriques^{2,3}, J. Fernández-Rossier^{3*}

¹ *Departamento de Física Aplicada, Universidad de Alicante, 03690 San Vicente del Raspeig, Spain*

² *Universidade de Santiago de Compostela, 15782 Santiago de Compostela, Spain and*

³ *International Iberian Nanotechnology Laboratory (INL),*

Av. Mestre José Veiga, 4715-330 Braga, Portugal

(Dated: March 7, 2025)

The AKLT Hamiltonian is a particular instance of a general class of model Hamiltonians defined in lattices with coordination z where each site hosts a spins $S = z/2$, interacting both with linear and non-linear exchange couplings. In two dimensions, the AKLT model features a gap in the spectrum, and its ground state is a valence bond solid state; that is an universal resource for measurement based quantum computing, motivating the quest of physical systems that realize this Hamiltonian. Given a finite-size system described with a specific instance of this general class of models, we address the question of how to asses if such system is a realization of the AKLT model using inelastic tunnel spectroscopy implemented with scanning tunnel microscopy (IETS-STM). We propose two approaches. First, in the case of a dimer, we show how to leverage non-equilibrium IETS-STM to obtain the energies of all excited states, and determine thereby the magnitude of both linear and non-linear exchange interactions. Second, we explore how IETS can probe the in-gap excitations associated to edge spins. In the AKLT limit, spins $S = 3/2$ at the edge of the lattice have coordination 2, giving rise to $S = 1/2$ dangling spins that can be probed with IETS. We propose a $S = 1/2$ effective Hamiltonian to describe the interactions between these dangling spins in the neighborhood of the AKLT point, where their degeneracy lifted.

I. INTRODUCTION

Quantum computing hinges on certain quantum states that make it possible to solve a variety of important problems¹ outperforming classical hardware. There are two complementary strategies for the generation of these resourceful quantum states. In the gate-based quantum computing approach, quantum algorithms are a prescribed sequence, most often very long, of quantum gates acting on one and two qubits at a time, starting from an initial unentangled product state. In this strategy, the system is driven out of equilibrium. In measurement-based quantum computing² (MBQC), the initial state is entangled in a special way, that makes it possible to implement quantum algorithms combining single-qubit gates and readouts, without having to use two-qubit gates. Importantly, the ground state of some Hamiltonians, such as the AKLT model in two dimensions^{3,4}, belong to this class of initial entangled states and therefore said to be universal resources⁵ for MBQC. In addition, it was demonstrated that the AKLT model is gapped in two dimensions^{6,7}. Therefore, if it were possible to engineer a physical system so that it realizes the two-dimensional AKLT model, and at a temperature significantly smaller than the gap, such system would spontaneously provide a very good starting point for MBQC.

AKLT models^{3,4,8} are particular instances of a general class of model Hamiltonians describing spins $S = z/2$ interacting both with linear and non-linear exchange couplings, in lattices with coordination number z . The wave function of the ground state can be written explicitly as a valence bond solid state: in every physical site, the spin S is represented by means of z virtual spins $S = 1/2$. At each bond between two physical sites, a singlet is formed

between two virtual spins. Furthermore, the wave function is symmetrized at each physical site, to ensure that the z virtual spins $1/2$ realize a physical spin S . In systems with periodic boundary conditions, the ground state is unique. In contrast, in systems with boundaries, the edge physical spins have dangling virtual spins, giving rise to a degeneracy of the ground state that can be interpreted in terms of emergent fractional $S = 1/2$ degrees of freedom. This constitutes a canonical example of fractionalization.

For spin chains³, the AKLT model is given by the bilinear-biquadratic (BLBQ) Hamiltonian with $S = 1$:

$$H_{BLBQ} = J \left(\sum_i \vec{S}_i \cdot \vec{S}_{i+1} + \beta (\vec{S}_i \cdot \vec{S}_{i+1})^2 \right) \quad (1)$$

with $\beta = \frac{1}{3}$. The most important properties of the one-dimensional AKLT model are the gap in the excitation spectrum, the symmetry protected topological order⁹ and the existence of fractional $S = 1/2$ edge excitations in open-end chains, shared¹⁰ by the BLBQ family in all points between $\beta = 0$, the Heisenberg model, and the AKLT point $\beta = 1/3$. These properties define the Haldane phase and have been observed experimentally in a number of systems, including crystals with decoupled spin chains¹¹, cold-atoms¹² and, important for this work, artificial one-dimensional $S = 1$ triangule lattices¹³. Whereas these systems provide a unique arena to explore fractionalization and to test the Haldane prediction¹⁴, the ground state of the Haldane phase of the BLBQ model is a universal resource to implement 1-qubit gates only⁵ and, therefore, they do not provide a viable alternative to gate-based quantum computing.

The simplest version of the AKLT model in 2D is realized in a honeycomb lattice⁴, where $z = 3$ and

$S = 3/2$. The AKLT is a special instance of the bilinear-biquadratic-bicubic (BLBQBC) Hamiltonian:

$$H_{BLBQBC} = J_1 \left(\sum_{\langle i, i' \rangle} \sum_{n=1}^3 \beta_n (\vec{S}_i \cdot \vec{S}_{i'})^n \right) \quad (2)$$

where i runs over the sites of the lattice, i' runs over the first neighbours of i and J_1 is the magnitude of the linear exchange (we consider $\beta_1 = 1$). The relative magnitude of non-linear exchange couplings is controlled by the parameters β_2, β_3 . The AKLT point⁴, for which the AKLT state is the ground state of Hamiltonian (2), is reached when $\beta_2 = \frac{116}{243}, \beta_3 = \frac{16}{243}$. We refer to the region in the β_2, β_3 plane that contains the AKLT point and has the same key properties ($S = 0$ ground state, gap in the excitation spectrum, fractional edge spins), as the AKLT phase. In contrast with the 1D case, very few papers have explored theoretically the boundaries of the AKLT phase in 2D¹⁵⁻¹⁷. Also in contrast with the one-dimensional case, so far no physical system has been found that realizes the AKLT phase in two dimensions. Promising physical platforms to make this happen would be multi-orbital Mott insulators¹⁸ and, given the successful precedent of $S = 1$ Haldane chains, lattices of $S = 3/2$ nanographenes^{19,20}.

The present work is inspired by the experimental approach that has been successful in the exploration of the 1D Haldane phase both in artificial chains made of $S = 1$ nanographenes¹³ as well as in the dimerized $S = 1/2$ chains²¹. In these works, the use of inelastic electron tunnel spectroscopy (IETS) carried out with scanning tunnel microscope (STM), was instrumental to measure the Haldane gap and the in-gap excitations associated to fractional spins at the edges, as anticipated theoretically²² and, in the $S = 1$ case¹³, to determine the presence of a significant non-linear exchange, $\beta \simeq 0.09$, that has been later accounted for theoretically²³. The fabrication of small two-dimensional lattices of $S = 3/2$ nanographenes²⁴, for which finite non-linear exchange parameters have been computed¹⁹ is a step toward the realization of a physical system that realizes the two-dimensional AKLT phase.

Here we address the question of how to certify, using STM-IETS, if a given on-surface spin system, including in particular a $S = 3/2$ nanographene crystal provides the physical realization of the AKLT phase. Our work can be framed in the more general context of how to probe neutral excitations in quantum insulators²⁵. We focus on two different problems. First, how to infer the parameters of the BLBQBC Hamiltonian using STM-IETS in a dimer. Second, we model the IETS-STM of the in-gap edge spin excitations in a hexamer of $S = 3/2$ described by the BLBQBC model. These in-gap states are expected in the AKLT point and its neighborhood and are akin to the extensively studied edge states in Haldane spin chains. Our results stress the advantages of studying small lattices to infer the spin couplings, as well as using the in-gap edge states as a smoking gun for the

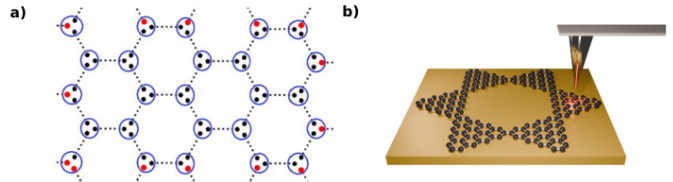


FIG. 1. a) Honeycomb lattice with $S = 3/2$. The edge states are shown in red. b) Schematic representation of a STM-IETS in a small cluster of $N = 6$.

AKLT phase. The feasibility of this approach is backed up by the experimental capability to fabricate and probe small artificial spin lattices, such as spin dimers^{26,27} and hexamers^{13,28}, as well as other structures like $S = 1/2$ spin chains^{21,29}. This bottom-up approach could be the way to avoid the trouble identifying the AKLT phase in macroscopically large systems, a problem well illustrated in the field of Kitaev materials³⁰.

The rest of this paper is organized as follows. In section II we review our methods. In section III we show the non-equilibrium IETS of a $S = 3/2$ dimer described with the BLBQBC Hamiltonian. Next, in section IV we explore the equilibrium IETS of an hexamer of $S = 3/2$ described with the BLBQBC model, both at the AKLT point and in the neighborhood. At last, in section V we present our final remarks.

II. METHODS

In this work we will be considering both dimers and hexamers of spins $3/2$, both because triangulene dimers and hexamers with $S = 1$ ^{13,26,28} and with $S = 1/2$ ^{29,31} have been reported, and also because the small size of these systems allows for an exact numerical diagonalization (ED) of the BLBQBC Hamiltonian. In order to study the role of edge states in the AKLT phase, we consider several types of *boundary* conditions, that differ by the number of *passivated* edges of the hexamer. In the AKLT point, every spin with coordination $(3 - n)$ has n *dangling* spin $S = 1/2$ that do not form a singlet.

Reference values for β_2, β_3 which are relevant in this work are shown in the table. Specifically, we consider two $S = 3/2$ molecules, the 4-triangulene (4T)¹⁹, a triangular shape nanographene molecules with 4 benzene rings along its side, and the 5-aza triangulene (5AT) a triangulene with 5 benzene rings along its side, where the central carbon atom was replaced by a nitrogen one³²⁻³⁷. Our calculations of β_2, β_3 for 4T¹⁹ the 5AT (see Appendix A) use the same approach¹³ that successfully accounts for non-linear exchange for $S = 1$, namely, exact diagonalization of the Hubbard models in a restricted space of multielectronic configurations, and the mapping of the low energy levels to a spin Hamiltonian.

Inelastic electron scanning tunneling microscopy can

System	β_2	β_3	J_1 (meV)
AKLT model ⁴	$\frac{116}{243}$	$\frac{16}{243}$	
$S = 3/2$ triangulenes ¹⁹	0.09	0.007	11.3
5-aza triangulene (see appendix)	0.27	0.034	10.6

TABLE I. Relevant reference values for β_2 and β_3 considered in this work.

probe the energy excitations of a single surface spin³⁸ through spin-flip assisted tunneling^{39–41}, where transport electrons exchange spin and energy with the atomic spin (Fig. 1 b). As electrons tunnel from tip to surface (or vice-versa), they can release their excess energy eV to excite the on-surface spins. The process has to conserve energy, so that $|eV| = E_M - E_{M'}$, where $E_M, E_{M'}$ are the energies of eigenstates of the on-surface spin Hamiltonian, the BLBQBC model in our case. Hence, as the bias is ramped up, with either sign, new transport inelastic channels open, which results in step-wise increase of the conductance, dI/dV . Since the total spin has also to be conserved, and the tunneling electron can either conserve its spin or flip, we have $|S_M - S_{M'}| = 0, 1$.

We compute the dI/dV treating the Kondo exchange that induces spin-flip inelastic tunneling between tip and sample to second order in perturbation theory^{22,39,4239}. In this approach, the dI/dV depends both on the occupations P_M of the eigenstates of the spin Hamiltonian, $|M\rangle$, and on the spin matrix elements $\langle M|S_a(i)|M'\rangle$ where $S_a(i)$ is the spin operator on the spin site i being excited with the STM tip and $a = x, y, z$. We compute the occupations P_M in two different approximations. First, equilibrium, valid at low current, where P_M is described by the Boltzmann function. At low temperatures, the only occupied state is the ground state, so that IETS is probing transitions from the ground-state only. This gives rise to thermally broadened step-like dI/dV curves. This approximation is justified as long as the spin relaxation time of the on-surface spin states is much shorter than the time elapsed between inelastic tunnel events, controlled by the current intensity, that in turn can be controlled with the tip-surface distance.

Here we are interested in probing transitions from excited states too, so that we have to consider the high-current regime, where the on-surface spins do not relax before the next inelastic excitation event takes place. In that regime, occupations are bias dependent and, more important, excitations from excited states can also be seen in the dI/dV , as shown experimentally for Mn dimers on Cu_2N ⁴³. The non-equilibrium kinetics of the the occupations of the collective spin states of the molecules is governed by the Pauli master equation⁴²:

$$\frac{dP_M}{dt} = \sum_{M'} P_{M'} W_{M',M} - P_M \sum_{M'} W_{M,M'} \quad (3)$$

where $W_{M',M}$ are the transition rates from M' to M . Here we assume that these rates are given by the Kondo exchange interactions, including both the events where

the electrons scatter between tip and sample and events where the electrons scatter between states in the same electrode. Expressions for $W_{M,M'}$ in terms of the spin matrix elements, are given in the appendix. Equation (3) is solved numerically using Runge-Kutta method. The resulting dI/dV lineshapes depart from the thermally broadened steps, on account of the bias dependence of the occupations, and result in overshoots at the inelastic step transitions. More importantly, the non-equilibrium dI/dV feature inelastic steps associated to transitions between excited states. These features provide additional information about the energy levels, and thereby the Hamiltonian parameters.

III. CHARACTERIZATION OF THE SPIN COUPLINGS BY IETS

In this section we discuss how to determine the three exchange couplings of the BLBQBC interaction in a non-equilibrium IETS experiment on a dimer. This would allow to determine how close a given system is of realizing the AKLT Hamiltonian. Before we present the method with some detail, we discuss the energy spectrum of the BLBQBC dimer.

A. Phase diagram of the BLBQBC dimer

Expressing the $\vec{S}_1 \cdot \vec{S}_2$ operator in terms of the total spin operator, it is straightforward to obtain the analytical expression for the energy levels of the BLBQBC dimer:

$$E(S_T) = \frac{J_1}{2} \mathcal{F}(S_T) + \frac{J_2}{4} \mathcal{F}(S_T)^2 + \frac{J_3}{8} \mathcal{F}(S_T)^3. \quad (4)$$

where $\mathcal{F}(S_T) = [S_T(S_T + 1) - \frac{15}{2}]$, and $S_T = 0, 1, 2, 3$ are the eigenvalues that the total spin operator of two spins $S = 3/2$ can take. Thus, the dimer spectrum features, at zero magnetic field, four different multiplets, labelled with S_T .

Interestingly the spin of the ground state can take three different values, $S = 0, 1, 2$ in the region where both β_2, β_3 are positive, and first neighbour exchange is antiferromagnetic. In the Heisenberg point ($\beta_2 = \beta_3 = 0$) the spin of the ground state is of course $S = 0$, on account of the antiferromagnetic nature of exchange. In contrast, in the AKLT point, the ground state has a nine-fold degeneracy containing spins $S = 0, 1, 2$; this can also be interpreted based on the emergence of an effective $S = 1$ at each site, resulting from the ferromagnetic coupling of pairs of dangling virtual spin-1/2. In Fig. 2 we show the gap between the ground state and first excited state of the spin models as a function of β_2, β_3 . This diagram defines three regions with different ground state spin; these three regions meet at the AKLT point. Marked with a star is the point in the phase diagram where a dimer made out of two nitrogen doped [5]-triangulenes (Aza[5]-triangulene) falls. Details on how these parameters were

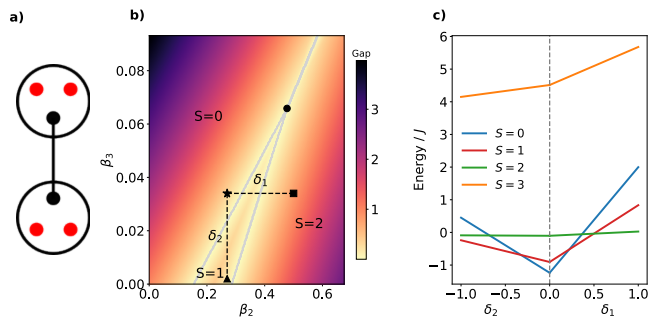


FIG. 2. a) Scheme of BLBQBC dimer, where the red dots represent the dangling virtual spins. b) Phase diagram for the BLBQBC dimer, where the color map represents the magnitude of the gap as a function of β_2, β_3 . We can find three regions, where the spin S of the ground state is $S = 0, 1, 2$. These three regions intersect in the AKLT point. c) Energies of the multiplets going through paths δ_1 and δ_2 . Here we can see how the energy changes when exploring the three different regimes of the phase diagram.

obtained for this particular system are given in Appendix B. Interestingly, we see that for this system β_2 is large enough as to have $S = 1$ as the ground state, but the size of β_3 takes it out of that region. Hence, it is not unlikely that similar nanographene systems will be found where the dimer ground state will be different from $S = 0$.

B. Finding exchange values using IETS

As we have seen before, the BLBQBC dimer has 4 multiplets ($S = 0, 1, 2, 3$), and thus three energy gaps. Here we will see how the parameters of the spin model can be experimentally obtained using IETS. First, in Fig. 3 we show in black the dI/dV curves as a function of the applied bias using perturbation theory up to 2nd order, in the three regions of the H_{BLBQBC} phase diagram. In panel a), where the ground state is a singlet, we find a single excitation step, associated to a singlet to a triplet transition. In panel b), because the ground state has $S = 1$, we have an excitation step associated with the triplet-to-singlet transition, and then another step due to excitation of the $S = 2$ manifold. Finally, in panel c) where the ground state is $S = 2$, we find again two steps stemming from $S = 2$ to $S = 1$ and to $S = 3$ transitions. From these dI/dV plots, we see that we have at most two excitation steps. However, since the spin model we are studying has three parameters, we would need three inelastic steps to be able to determine the three energy scales of the BLBQBC dimer experimentally.

With this in mind, we move on from the equilibrium dI/dV , and compute its non-equilibrium counterpart. In this case, the occupation of the states is driven out of equilibrium by, for example, increasing the conductance of the junction bringing the tip closer to the surface⁴³. This leads to more available spin excitations, and it might

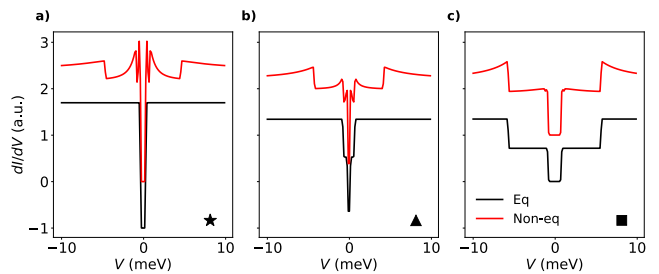


FIG. 3. dI/dV curves both for equilibrium IETS and non-equilibrium. The values used for the non-linear couplings of the BLBQBC model correspond to a) the aza-triangulene case with $\beta_2 = 0.27$ and $\beta_3 = 0.034$ (\star in Fig. 2), b) $\beta_2 = 0.27$ and $\beta_3 = 0.002$ (\blacktriangle) and c) $\beta_2 = 0.5$ and $\beta_3 = 0.034$ (\blacksquare). The parameters used for the simulations are shown in Appendix A.

become possible to probe enough steps to fully characterize the spin model. The observation of these three steps, at voltages V_I, V_{II}, V_{III} (see red lines in figure 3) would permit one to fully determine a system of three equations and three unknowns (J_1, J_2, J_3):

$$\begin{aligned} eV_I &= E(1) - E(0) = J_1 - \frac{13}{2}J_2 + \frac{511}{16}J_3 \\ eV_{II} &= E(2) - E(1) = 2J_1 - 7J_2 + \frac{163}{8}J_3 \\ eV_{III} &= E(3) - E(2) = 3J_1 + \frac{9}{2}J_2 + \frac{189}{16}J_3 \end{aligned} \quad (5)$$

where we have used $\mathcal{F}(0) = -\frac{15}{2}$, $\mathcal{F}(1) = -\frac{11}{2}$, $\mathcal{F}(2) = -\frac{3}{2}$ and $\mathcal{F}(3) = \frac{9}{2}$. We note that the excitations V_{II} and V_{III} are, very often, very close in energy. Therefore, in some cases, such as figure 3c, the two steps associated to them are almost degenerate, which will complicate this procedure.

IV. IETS OF $S = 3/2$ HEXAMER

In this section, we examine the $S = 3/2$ AKLT model in a small cluster of six spins forming a hexamer. This structure is among the smallest that allows for geometric intuition while remaining computationally feasible via exact diagonalization (ED). Our focus is on understanding the role of in-gap edge states within the AKLT phase. To this end, we consider two geometries, namely: (i) *open boundary conditions* (OBC), where the hexamer has an unpaired $S = 1/2$ edge spin at each site (Fig. 4a), and (ii) *periodic boundary conditions* (PBC), where the structure is "closed", passivating all edge spins and eliminating edge states.

A. Low energy states at the AKLT point

The AKLT wave function is built by describing each physical $S = 3/2$ with three virtual $S = 1/2$, each form-

ing a singlet with a virtual spin from a first neighbor. For the hexamer, all 6 sites have coordination two, so that all of them have one dangling virtual spin $1/2$ (red dots in Fig. 4a). This results in a ground state manifold with degeneracy $2^6 = 64$. We can also choose to introduce additional couplings among different pairs of spins in the hexamer, reducing thereby both the number of doubly-coordinated sites and the degeneracy of the ground state. For the case with periodic boundary conditions, with all edges passivated, the ground state is unique and has $S = 0$, and the lowest excited state has $S = 1$, with an excitation energy $\Delta E_{PBC} \simeq J/2$. The spectrum can be seen in the left side of Fig. 4c

In an hypothetical finite-size nanographene hexamer that realizes the AKLT Hamiltonian the 64 degenerate ground states include one septet ($S = 3$), five quintets ($S = 2$), nine triplets ($S = 1$), and five singlets ($S = 0$). The first excited state is now defined as the transition from this degenerate manifold to the 65th state, and has a value of $\Delta E_{OBC} \simeq 1.855J$. This excitation energy is considerably larger than the PBC case. Intriguingly, we note that the lowest-energy excited state of the OBC hexamer, i.e. state number 65, has $S = 4$. For PBC the first excited state has $S = 1$. We interpret the $S = 4$ state with OBC as a collective excitation with $S = 1$ over a ground state with $S = 3$, as if the collective excitation was mediating a ferromagnetic interaction among the dangling spins.

B. IETS in the AKLT limit

The inelastic electron tunneling spectroscopy (IETS) of a hexamer at the AKLT point is primarily dictated by the degeneracy of its ground state. With PBC there is a unique ground state and therefore transitions are only possible to excited states with $S = 0$ and $S = 1$. Our calculations show two dominant steps in that case. In contrast, with OBC, the ground state includes states with $S = 0, 1, 2, 3$, which increases dramatically the number of possible spin excitations, leading to a complex dI/dV spectrum with multiple inelastic steps associated (Fig.4b).

A crucial feature of the IETS spectrum of the hexamer in the AKLT point is that it shows a strong response to an external magnetic field. When a magnetic field is applied, the ground-state degeneracy is lifted due to Zeeman splitting. In the limit where $g\mu_B B \gg k_B T$, states with larger negative S_z become preferentially occupied. This has three main effects in the dI/dV spectrum: i) steps associated to transitions between the previously degenerate 64-state manifold appear; ii) the number of transitions to higher energy states is reducing significantly, since the ground state is now unique (with a given S and S_z quantum numbers), and spin selection rules only allow transitions with $\Delta S = 0, 1$; iii) the value of the conductance at zero bias increases. In fact, in the inset of Fig.4b we find an approximate linear dependence between the de-

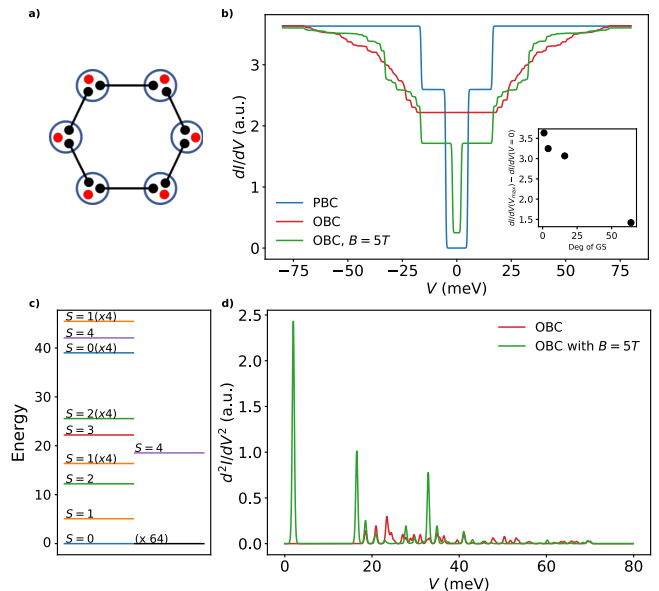


FIG. 4. a) Schematic representation of the AKLT hexamer. b) dI/dV curves. Inset: Difference between the high bias and zero bias value for different number of passivated edge states. c) Energy spectrum of the hexamer in the AKLT point for PBC (left) and OBC (right). d) d^2I/dV^2 of the OBC hexamer with and without magnetic field. For all results we have used $J = 10meV$.

generacy of the ground state and the conductance value at $V = 0$.

The difference between of the $B = 0$ and large B IETS spectra is better appreciated by representing d^2I/dV^2 (Fig.4d). Therefore, a smoking gun of the realization of the AKLT phase would be a very strong magnetic field dependence of the number of peaks in the IETS spectra in finite-size lattices, revealing the topological degeneracy of the ground state.

C. Effective spin model for fractional edge spins close to the AKLT point

We now discuss the spectrum of the OBC hexamer described with the BLBQBC model close to the AKLT point, so that the degeneracy of the GS is lifted, but there is still a clear gap between the 64 low energy states and the rest. In Fig. 5a, we present the energy spectrum of the BLBQBC model with parameters $\beta_2 = 0.4602$ and $\beta_3 = 0.0681$, chosen to be close to the AKLT point and in the red trajectory r shown in Fig. 5c. The eigenstates are classified according to their total spin S and wave vector k (see Appendix C). Very much like in the case of Haldane chains, here we interpret the splitting of the GS levels in terms of an *effective spin interactions* between the $S = 1/2$ fractional spins. We propose the following effective Hamiltonian, that includes linear exchange couplings up

to third-nearest neighbors:

$$H_L = \sum_{n=1,2,3} j_n \sum_i \vec{\sigma}_i \cdot \vec{\sigma}_{i\pm n}. \quad (6)$$

This Hamiltonian can be resolved analytically for the case with $j_2 = j_3$ ⁴⁴. For the general case, we find j_1, j_2, j_3 by numerical fitting. Specifically, we minimize the function:

$$\mathcal{E} = \sum_{S,k,\alpha} \left(E_{S,k}^{(3/2)}(\alpha) - E_{S,k}^{(1/2)}(\alpha, j_1, j_2, j_3) \right)^2 \quad (7)$$

where the sum over S and k includes the 20 multiplets of the subspace of dimension 2^6 discussed in the previous section and labeled with the correspondent k value, and α is the additional index to label different multiplets with the same S and k . The resulting spectrum, for $\beta_2 = 0.4602$ and $\beta_3 = 0.0681$, is shown in Fig. 5b. We see a perfect agreement between the spectra of the full $S = 3/2$ model and the effective model. Both models predict a ground state with $S = 0$ and $k = \pi$, a first excited state with $S = 1$ and $k = 0$ and a second excited state with $S = 2$ and $k = \pi$; as for the multiplets with higher energy one finds a perfect correspondence with the $S = 3/2$ model.

Further validation of the model comes from the fitting of the parameters j_1, j_2, j_3 as β_2 and β_3 are varied around the AKLT points, in two circular trajectories in the (β_2, β_3) plane, centered around the AKLT point, with radius $r = 0.05, R = 0.1$, parametrized by $\theta \in (0, 2\pi)$. Our results show a smooth evolution of $j_i(\theta)$, both for r and R . We note that the effective exchange interaction is smaller for the smallest radius r , as expected, given that the effective couplings should vanish at the AKLT point. Importantly, the j_i couplings can take both positive and negative values, describing antiferromagnetic (AF) and ferromagnetic (FM) interactions, respectively.

The excursion in the (β_2, β_3) plane visits two regions with different spin S of the ground state, $S = 0$ and $S = 1$. The sign of the values obtained for j_1, j_2, j_3 provides insight to understand these two ground states. There is a segment within $0.6 \lesssim \theta \lesssim 3.7$ where j_1 and j_3 are AF, whereas j_2 is FM, that clearly stabilizes Neel-type correlations, compatible with $S = 0$. On the contrary, out of this segment the signs of the 3 couplings are inverted, which results in frustration, and roughly correspond to the region where the ground state has $S = 1$. In the proximity of the AKLT point where we are studying the system, the 65th state still has $S = 4$ and $k = \pi$, and the big gap with the bulk of low-energy states is also maintained.

V. CONCLUSIONS

We have developed a theoretical framework to guide experimental efforts in realizing the AKLT model using nanographene-based structures. By characterizing

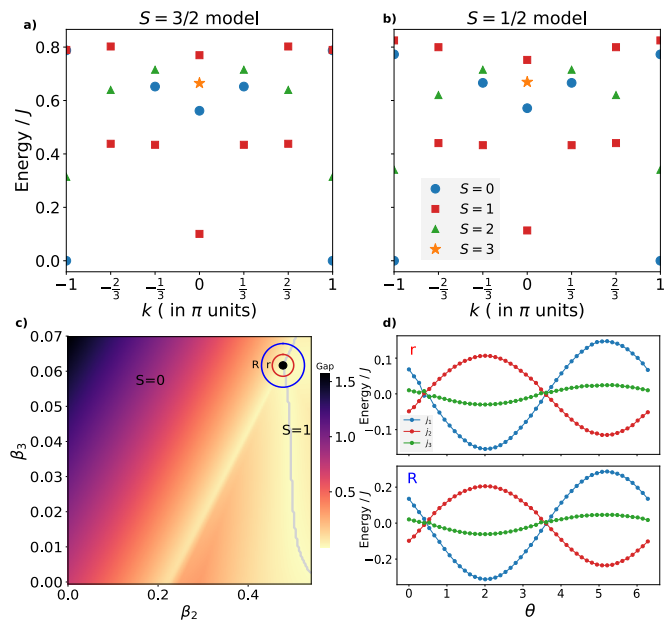


FIG. 5. Effective model. a) and b) Comparison of the spectra of the $S = \frac{3}{2}$ model with the effective $S = \frac{1}{2}$ model. The multiplets have been labeled by their S_{tot} and in the x -axis we show their k value. c) Value of the gap for different values of β_2 and β_3 in the BLBQBC model. In comparison with the dimer case, here we can only get a ground state with $S = 1$ but not with $S = 2$. d) Fitting of the values of j_1, j_2 and j_3 for the effective model for values of β_2 and β_3 around the AKLT point in two different trajectories with $r = 0.05$ and $R = 0.1$.

the exchange couplings and predicting observable features of the AKLT phase, we highlight the crucial role of emergent fractional edge spins in understanding the system's low-energy physics. For the BLBQBC dimer, we show that the spin of the ground state can take different values ($S = 0, 1, 2$) depending on the values of β_2 and β_3 , demonstrating the system's tunability of the system, where small variations in interaction parameters can lead to qualitative changes in the ground state and, consequently, in the excitation spectrum. Additionally, we propose a method to extract nonlinear exchange parameters using non-equilibrium inelastic electron tunneling spectroscopy (IETS), enabling full characterization of the spin Hamiltonian through differential conductance measurements.

Extending our analysis to an hexamer in the $S = 3/2$ AKLT model, we predict a strong dependence of the IETS spectrum on an external magnetic field, leading to ground-state degeneracy lifting and therefore the appearance of inelastic transition within the low-energy manifold, and suppression of high-energy excitations due to preferential occupation of states with large negative S_z . Near the AKLT point, the 64-fold ground-state degeneracy is lifted and the system can be described by effective interactions between fractional $S = 1/2$ edge spins, which we model using an effective spin Hamiltonian incorpo-

rating up to third-nearest-neighbor interactions. An intriguing feature of the hexamer's excitation spectrum is the $S = 4$ state (state 65), which persists as the system moves away from the AKLT point. This state can be interpreted as a collective excitation mediating an effective ferromagnetic interaction among the dangling edge spins, contrasting with the periodic boundary condition (PBC) case, where the first excited state has $S = 1$. Future studies should extend these methods to larger nanographene structures, leveraging advanced numerical techniques like Quantum Monte Carlo⁴⁵ and Neural-Network Quantum States⁴⁶ to further explore AKLT physics in realistic experimental settings, with implications for quantum magnetism and measurement-based quantum computing⁸.

ACKNOWLEDGEMENTS

JFR acknowledges Nils Krane for conversations in the early stage of this project. MFC acknowledges funding from Generalitat Valenciana (CIACIF/2021/434). J.F.-R. and J.C.G.H. acknowledge financial support from SNF Sinergia (Grant Pimag), FCT (Grant No. PTDC/FIS-MAC/2045/2021), the European Union (Grant FUNLAYERS - 101079184). J.F.-R. acknowledges funding from Generalitat Valenciana (Prometeo2021/017 and MFA/2022/045) and MICIN-Spain (Grants No. PID2019-109539GB-C41 and PRTR-C1y.I1)

Appendix A: Calculation of dI/dV

For the sake of completeness, we review the formalism to calculate dI/dV that we have used, that follows previous work by one of us^{39,42}. The starting point is a Hamiltonian for free fermions in the tip and the surface, and a spin Hamiltonian, the BLBQBC model in this paper, for the on-surface spins. The otherwise free fermions are coupled to the on-surface spins via a Kondo exchange that has an additional degree of freedom (tip/sample). Therefore, there are 4 Kondo couplings, attending two the initial and final electrode of a given process: tip-tip (TT), tip-sample (TS), sample-tip (ST), sample-sample (SS). Only ST and TS processes contribute to the spin-flip tunnel current. TT and SS process play a role in the dissipative spin dynamics of the on-surface spins, relevant for the non-equilibrium calculation.

The inelastic current can be computed as^{39,42} the sum over initial states M of the product of their occupations P_M times the sum over final states M' , weighted by the spin matrix elements

$$I \propto \sum_{M,M'} P_M(V) i_-(\Delta_{M,M'} + eV) \times \sum_{\eta,\eta'} |\mathbf{S}_{\mathbf{a},\eta,\eta'}^{\mathbf{M},\mathbf{M}'}|^2 \quad (\text{A1})$$

where η and η' are the electrodes labels, T for tip and S

for surface, and

$$\mathbf{S}_{\mathbf{a},\eta,\eta'}^{\mathbf{M},\mathbf{M}'} \equiv \frac{1}{\chi} \sum_{i,a=x,y,z} \nu_\eta(i) \nu_{\eta'}(i) \langle M | S_a(i) | M' \rangle. \quad (\text{A2})$$

The dimensionless factors $\nu_\eta(i)$ code the intensity of the coupling of tip and sample to the different sites i in a given spin lattice⁴². Therefore, the site dependence of the inelastic current is encoded in the ν parameters. We also define a normalization factor $\chi = \sum_i \nu_T(i) \nu_S(i)$ is a parameter that quantifies the tip-surface transmission through the magnetic atoms. The function i_- is given by⁴²:

$$i_-(\Delta + eV) = \frac{G_0}{e} [\mathcal{G}(\Delta + eV) - (\Delta - eV)] \quad (\text{A3})$$

and $G_0 = \frac{e^2}{h}$ with $\mathcal{G}(\omega) \equiv \omega (1 - e^{-\beta\omega})^{-1}$. Using Eq. (A1), the calculation of dI/dV gives thermally broadened steps at the bias voltages that match on-surface excitations that conserve energy and spin. The intensity of the steps is controlled by the spin matrix elements.

In our simulations for the non-equilibrium kinetics of the spin dimer, we take into account Kondo exchange interactions up to second order in perturbation theory. Kondo exchange includes not only the spin and the momentum of the itinerant electrons but also an index for the electrode. Therefore, for the calculation of the spin relaxation and excitation rates we consider⁴² scattering events where the initial and final states of the electron can be in two electrodes. As a result, there are 4 types of event, tip-tip, surface-surface, surface-tip, and tip-surface. For a given sign of bias, only the tip-surface events contribute to the excitation of the spin towards higher energy states. The tip-tip and surface-surface scattering events contribute to the relaxation of the system, promoting the occupation of low energy states. The scattering rates depend on how the two sites of the dimer are coupled to tip and substrate. We assume that the Kondo coupling to the substrate is not the same for the two spins in order to have finite spin relaxation rates⁴⁷. The expression for the rates that enter the master equation reads:

$$W_{M,M'}^{\eta,\eta'} = \frac{2\pi T^2}{h} \mathcal{G}(\Delta + \mu_\eta - \mu_{\eta'}) \frac{\rho_\eta \rho_{\eta'}}{4} \sum_n |\mathbf{S}_{\mathbf{a},\eta,\eta'}^{\mathbf{M},\mathbf{M}'}(n)|^2 \quad (\text{A4})$$

where T gives the magnitude of the exchange coupling of the atomic spin to the transport electrons, $\mu_\eta - \mu_{\eta'}$ is the voltage difference of the electrodes and ρ_η is the density of states at the Fermi Energy for the electrode η .

For the simulation, we took the following parameters: temperature $T = 0.05K$, magnetic field $B = 0$, the dimensionless coupling to tip of $\nu_S(1) = \nu_S(2) = 1.5$, $\nu_T(1) = 2.5$, $\nu_T(2) = 1.5$ and $\rho_T = \rho_S = 0.1$.

Appendix B: Spin model parameters for the Aza[5]-Triangulene dimer

In the main text, we considered as a reference value for the H_{BLBQBC} parameters the ones of an Aza[5]-Triangulene dimer, $\beta_2 = 0.27$ and $\beta_3 = 0.034$. In this appendix, we shall briefly explain how these values were obtained.

The Aza[5]-Triangulene (A5T) refers to a triangulene with five benzene rings along its side, where the central carbon atom was replaced by a nitrogen one³²⁻³⁷. To model this molecule, we use a Hubbard model with first and third neighbor hopping, and an on-site potential on the nitrogen site and its nearest neighbors. A similar procedure has been used in Refs.^{19,48}, showing results in excellent agreement with density functional theory (DFT). Based on those works we consider the first and third neighbor hoppings to be $t = -2.7\text{eV}$ and $t_3 = t/10$, respectively, the Nitrogen on-site potential to be $V_0 = -4\text{ eV}$ (and $V_1 = -0.85\text{ eV}$ on the first neighboring sites) and we take the Hubbard repulsion parameter as $U = |t|$. Without nitrogen functionalization, in the non-interacting limit, the 5T molecule has 4 orbitals at zero energy⁴⁹, each hosting one electron, leading to a spin $S = 2$ when interactions are accounted for. However, when the central carbon atom is replaced by nitrogen, one of these zero energy levels goes down in energy, due to the electrostatic potential created by the extra proton in nitrogen, compared to carbon. This red-shifted zero mode becomes doubly occupied due to the additional electron brought in by the dopant; the other three levels at zero energy remain singly occupied, so that the ground state of A5T has $S = 3/2$. The A5T dimer is simply obtained by covalent coupling two of these systems tip to tip. Our calculations for the dimer predict a $S = 0$ ground state, with a set of low energy excitations well described by the spin-3/2 H_{BLBQBC} Hamiltonian.

To obtain the values of the exchange interactions, we use a similar procedure to the one used in Refs.^{19,48}. First, we solve the fermionic Hubbard model in the configuration interaction approach using the complete active space approximation (CI-CAS). Afterwards, we fit the energies of the spin model to the energies found from the fermionic model, allowing us to find the values of exchange one should use. The CI-CAS method can be

summarized as follows: first, one solves the single particle problem (i.e. without Hubbard repulsion); second, the Hubbard Hamiltonian is expressed in the basis of the eigenstates found in the previous step; finally, we truncate the Hilbert space to include only the single particle states closer to zero-energy, and diagonalize the resulting Hamiltonian in the Hilbert space spanned by all possible electron configurations over the considered single particle states.

Appendix C: Classification of hexamer states using C_6 symmetry

We discuss the method to label the states of hexamers with a wave vector, taking advantage of the fact that hexamer Hamiltonians have C_6 symmetry. We adopt the following procedure. First, we build the translation operator, in terms of swap operators:

$$C_6^S = \prod_{i=0}^4 \mathcal{S}_{i,i+1}^{(S)}. \quad (\text{C1})$$

where $\mathcal{S}_{i,i+1}^{(S)}$ is the swap operator for spin S . This operator satisfies the equation $C_6^S |k\rangle = e^{ik} |k\rangle$, where $k = \pi n/6$, with $n = 0, \pm 1, \pm 2, 3$. Generalization for L sites is straightforward, the upper limit on the product should be $L - 2$ instead, and k should take the values $\pi n/L$ with $n = 0, 1, \dots, L - 1$.

For $S = 1/2$ the swap operators is:

$$\mathcal{S}_{ij}^{(1/2)} = \left(\frac{1}{2} + 2\vec{S}_i \cdot \vec{S}_{i+1} \right)$$

For $S = 3/2$, the swap operator adds quadratic and cubic terms and reads:

$$\mathcal{S}_{ij}^{(3/2)} = -\frac{67}{32} - \frac{9}{8}(S_i \cdot S_j) + \frac{11}{18}(S_i \cdot S_j)^2 + \frac{2}{9}(S_i \cdot S_j)^3$$

The numerical diagonalizations of the hexamer Hamiltonians yield manifolds with degeneracies larger than those imposed by the spin symmetry. We represent the translation operator in the basis of such manifolds and diagonalize it, obtaining thereby simultaneous eigenvectors of the Hamiltonian and the translation operator, with well defined wave vector k .

* On permanent leave from Departamento de Física Aplicada, Universidad de Alicante, 03690 San Vicente del Raspeig, Spain.

¹ Alexander M Dalzell, Sam McArdle, Mario Berta, Przemyslaw Bienias, Chi-Fang Chen, András Gilyén, Connor T Hann, Michael J Kastoryano, Emil T Khabiboulline, Aleksander Kubica, *et al.*, “Quantum algorithms: A survey of applications and end-to-end complexities,” arXiv preprint arXiv:2310.03011 (2023).

² Robert Raussendorf, Daniel E Browne, and Hans J

Briegel, “Measurement-based quantum computation on cluster states,” Physical review A **68**, 022312 (2003).

³ Ian Affleck, Tom Kennedy, Elliott H. Lieb, and Hal Tasaki, “Rigorous results on valence-bond ground states in antiferromagnets,” Phys. Rev. Lett. **59**, 799–802 (1987).

⁴ Ian Affleck, Tom Kennedy, Elliott H Lieb, and Hal Tasaki, “Valence bond ground states in isotropic quantum antiferromagnets,” Communications in Mathematical Physics **115**, 477–528 (1988).

⁵ Tzu-Chieh Wei, Ian Affleck, and Robert Raussendorf,

- “Affleck-kennedy-lieb-tasaki state on a honeycomb lattice is a universal quantum computational resource,” *Phys. Rev. Lett.* **106**, 070501 (2011).
- 6 Nicholas Pomata and Tzu-Chieh Wei, “Demonstrating the affleck-kennedy-lieb-tasaki spectral gap on 2d degree-3 lattices,” *Physical review letters* **124**, 177203 (2020).
 - 7 Marius Lemm, Anders W. Sandvik, and Ling Wang, “Existence of a spectral gap in the affleck-kennedy-lieb-tasaki model on the hexagonal lattice,” *Phys. Rev. Lett.* **124**, 177204 (2020).
 - 8 Tzu-Chieh Wei, Robert Raussendorf, and Ian Affleck, “Some aspects of affleck–kennedy–lieb–tasaki models: Tensor network, physical properties, spectral gap, deformation, and quantum computation,” *Entanglement in Spin Chains: From Theory to Quantum Technology Applications*, 89–125 (2022).
 - 9 Frank Pollmann, Erez Berg, Ari M. Turner, and Masaki Oshikawa, “Symmetry protection of topological phases in one-dimensional quantum spin systems,” *Phys. Rev. B* **85**, 075125 (2012).
 - 10 U Schollwöck, Th Jolicoeur, and Th Garel, “Onset of incommensurability at the valence-bond-solid point in the $s = 1$ quantum spin chain,” *Physical Review B* **53**, 3304 (1996).
 - 11 M. Hagiwara, K. Katsumata, Ian Affleck, B. I. Halperin, and J. P. Renard, “Observation of $s = 1/2$ degrees of freedom in an $s = 1$ linear-chain Heisenberg antiferromagnet,” *Phys. Rev. Lett.* **65**, 3181–3184 (1990).
 - 12 Pimonpan Sompet, Sarah Hirthe, Dominik Bourgund, Thomas Chalopin, Julian Bibo, Joannis Koepsell, Petar Bojović, Ruben Verresen, Frank Pollmann, Guillaume Salomon, *et al.*, “Realizing the symmetry-protected haldane phase in fermi-hubbard ladders,” *Nature* **606**, 484–488 (2022).
 - 13 Shantanu Mishra, Gonçalo Catarina, Fupeng Wu, Ricardo Ortiz, David Jacob, Kristjan Eimre, Ji Ma, Carlo A Pignedoli, Xinliang Feng, Pascal Ruffieux, Joaquin Fernandez-Rossier, and Roman Fasel, “Observation of fractional edge excitations in nanographene spin chains,” *Nature* **598**, 287–292 (2021).
 - 14 F. D. M. Haldane, “Continuum dynamics of the 1-D Heisenberg antiferromagnet: Identification with the O(3) nonlinear sigma model,” *Physics Letters A* **93**, 464–468 (1983).
 - 15 R. Ganesh, D. N. Sheng, Young-June Kim, and A. Paramakanti, “Quantum paramagnetic ground states on the honeycomb lattice and field-induced néel order,” *Phys. Rev. B* **83**, 144414 (2011).
 - 16 Artur Garcia-Saez, Valentin Murg, and Tzu-Chieh Wei, “Spectral gaps of affleck-kennedy-lieb-tasaki hamiltonians using tensor network methods,” *Physical Review B* **88**, 245118 (2013).
 - 17 Ching-Yu Huang, Xie Chen, and Feng-Li Lin, “Symmetry-protected quantum state renormalization,” *Phys. Rev. B* **88**, 205124 (2013).
 - 18 Maciej Koch-Janusz, D. I. Khomskii, and Eran Sela, “Affleck-kennedy-lieb-tasaki state on a honeycomb lattice from t_{2g} orbitals,” *Phys. Rev. Lett.* **114**, 247204 (2015).
 - 19 Gonçalo Catarina, João CG Henriques, Alejandro Molina-Sánchez, António T Costa, and Joaquín Fernández-Rossier, “Broken-symmetry magnetic phases in two-dimensional triangulene crystals,” *Physical Review Research* **5**, 043226 (2023).
 - 20 João Henriques, Mar Ferri-Cortés, and Joaquín Fernández-Rossier, “Designer spin models in tunable two-dimensional nanographene lattices,” *Nano Letters* **24**, 3355–3360 (2024).
 - 21 Chenxiao Zhao, Gonçalo Catarina, Jin-Jiang Zhang, João CG Henriques, Lin Yang, Ji Ma, Xinliang Feng, Oliver Gröning, Pascal Ruffieux, Joaquín Fernández-Rossier, *et al.*, “Tunable topological phases in nanographene-based spin-1/2 alternating-exchange heisenberg chains,” *Nature Nanotechnology*, 1–7 (2024).
 - 22 F Delgado, CD Batista, and J Fernández-Rossier, “Local probe of fractional edge states of $s = 1$ heisenberg spin chains,” *Physical Review Letters* **111**, 167201 (2013).
 - 23 João CG Henriques and Joaquín Fernández-Rossier, “Anatomy of linear and nonlinear intermolecular exchange in $s = 1$ nanographene,” *Physical Review B* **108**, 155423 (2023).
 - 24 Aidan Delgado, Carolin Dusold, Jingwei Jiang, Adam Cronin, Steven G Louie, and Felix R Fischer, “Evidence for excitonic insulator ground state in triangulene kagome lattice,” *arXiv preprint arXiv:2301.06171* (2023).
 - 25 Sanfeng Wu, Leslie M Schoop, Inti Sodemann, Roderich Moessner, Robert J Cava, and NP Ong, “Charge-neutral electronic excitations in quantum insulators,” *Nature* **635**, 301–310 (2024).
 - 26 Shantanu Mishra, Doreen Beyer, Kristjan Eimre, Ricardo Ortiz, Joaquín Fernández-Rossier, Reinhard Berger, Oliver Gröning, Carlo A Pignedoli, Roman Fasel, Xinliang Feng, *et al.*, “Collective all-carbon magnetism in triangulene dimers,” *Angewandte Chemie International Edition* (2020).
 - 27 Elia Turco, Annika Bernhardt, Nils Krane, Leosš Valenta, Roman Fasel, Michal Juričček, and Pascal Ruffieux, “Observation of the magnetic ground state of the two smallest triangular nanographenes,” *JACS Au* (2023).
 - 28 Jeremy Hieulle, Silvia Castro, Niklas Friedrich, Alessio Vegliante, Francisco Romero Lara, Sofia Sanz, Dulce Rey, Martina Corso, Thomas Frederiksen, Jose Ignacio Pascual, *et al.*, “On-surface synthesis and collective spin excitations of a triangulene-based nanostar,” *Angewandte Chemie International Edition* **60**, 25224–25229 (2021).
 - 29 Chenxiao Zhao, Lin Yang, João CG Henriques, Mar Ferri-Cortés, Gonçalo Catarina, Carlo A Pignedoli, Ji Ma, Xinliang Feng, Pascal Ruffieux, Joaquín Fernández-Rossier, *et al.*, “Gapless spin excitations in nanographene-based antiferromagnetic spin-1/2 heisenberg chains,” *arXiv preprint arXiv:2408.10045* (2024).
 - 30 Simon Trebst and Ciarán Hickey, “Kitaev materials,” *Physics Reports* **950**, 1–37 (2022).
 - 31 Nils Krane, Elia Turco, Annika Bernhardt, David Jacob, Guido Gandus, Daniele Passerone, Mathieu Luisier, Michal Juričček, Roman Fasel, Joaquin Fernández-Rossier, *et al.*, “Exchange interactions and intermolecular hybridization in a spin-1/2 nanographene dimer,” *Nano letters* **23**, 9353–9359 (2023).
 - 32 Khalid N Anindya and Alain Rochefort, “Controlling the magnetic properties of two-dimensional carbon-based kagome polymers,” *Carbon Trends* **7**, 100170 (2022).
 - 33 Rémy Pawlak, Khalid N Anindya, Outhmane Chahib, Jung-Ching Liu, Paul Hiret, Laurent Marot, Vincent Luzet, Frank Palmino, Frédéric Chérioux, Alain Rochefort, and Ernst Meyer, “On-surface synthesis and characterization of radical spins in kagome graphene,” *ACS nano* (2025).
 - 34 Manuel Vilas-Varela, Francisco Romero-Lara, Alessio Veg-

- liante, Jan Calupitan, Adrián Martínez, Lorenz Meyer, Unai Uriarte-Amiano, Niklas Friedrich, Dongfei Wang, Fabian Schulz, Natalia E. Koval, María E. Sandoval-Salinas, David Casanova, Martina Corso, Emilio Artacho, Diego Peña, and José Ignacio Pascual, “On-surface synthesis and characterization of a high-spin aza-[5]-triangulene,” *Angewandte International Edition Chemie* (2023).
- ³⁵ Tao Wang, Alejandro Berdonces-Layunta, Niklas Friedrich, Manuel Vilas-Varela, Jan Patrick Calupitan, Jose Ignacio Pascual, Diego Peña, David Casanova, Martina Corso, and Dimas G de Oteyza, “Aza-triangulene: On-surface synthesis and electronic and magnetic properties,” *Journal of the American Chemical Society* **144**, 4522–4529 (2022).
- ³⁶ James Lawrence, Yuanyuan He, Haipeng Wei, Jie Su, Shaotang Song, Alina Wania Rodrigues, Daniel Miravet, Pawel Hawrylak, Jianwei Zhao, Jishan Wu, *et al.*, “Topological design and synthesis of high-spin aza-triangulenes without jahn–teller distortions,” *ACS nano* **17**, 20237–20245 (2023).
- ³⁷ Hongde Yu and Thomas Heine, “Prediction of metal-free stoner and mott-hubbard magnetism in triangulene-based two-dimensional polymers,” *Science Advances* **10**, eadq7954 (2024).
- ³⁸ Andreas J Heinrich, Jay A Gupta, Christopher P Lutz, and Donald M Eigler, “Single-atom spin-flip spectroscopy,” *Science* **306**, 466–469 (2004).
- ³⁹ J. Fernández-Rossier, “Theory of single-spin inelastic tunneling spectroscopy,” *Phys. Rev. Lett.* **102**, 256802 (2009).
- ⁴⁰ Nicolás Lorente and Jean-Pierre Gauyacq, “Efficient spin transitions in inelastic electron tunneling spectroscopy,” *Physical review letters* **103**, 176601 (2009).
- ⁴¹ J Fransson, “Spin inelastic electron tunneling spectroscopy on local spin adsorbed on surface,” *Nano letters* **9**, 2414–2417 (2009).
- ⁴² F Delgado and J Fernández-Rossier, “Spin dynamics of current-driven single magnetic adatoms and molecules,” *Physical Review B* **82**, 134414 (2010).
- ⁴³ Sebastian Loth, Kirsten Von Bergmann, Markus Ternes, Alexander F Otte, Christopher P Lutz, and Andreas J Heinrich, “Controlling the state of quantum spins with electric currents,” *Nature Physics* **6**, 340–344 (2010).
- ⁴⁴ D. Kouzoudis, “Exact analytical partition function and energy levels for a heisenberg ring of $n=6$ spin $1/2$ sites,” *Journal of Magnetism and Magnetic Materials* **189**, 366–376 (1998).
- ⁴⁵ Anders W. Sandvik, “Computational studies of quantum spin systems,” *AIP Conference Proceedings* **1297**, 135–338 (2010).
- ⁴⁶ Giuseppe Carleo and Matthias Troyer, “Solving the quantum many-body problem with artificial neural networks,” *Science* **355**, 602–606 (2017).
- ⁴⁷ This is a shortcoming of the approximation of ignoring the Bloch phase in the Kondo coupling⁵⁰.
- ⁴⁸ João Henriques, David Jacob, Alejandro Molina-Sánchez, Gonçalo Catarina, António T Costa, and Joaquín Fernández-Rossier, “Beyond spin models in orbitally degenerate open-shell nanographenes,” *Nano Letters* **24**, 12928–12934 (2024).
- ⁴⁹ Joaquín Fernández-Rossier and J. J Palacios, “Magnetism in graphene nanoislands,” *Physical Review Letters* **99**, 177204 (2007).
- ⁵⁰ F Delgado and J Fernández-Rossier, “Rkky oscillations in the spin relaxation rates of atomic-scale nanomagnets,” *Physical Review B* **95**, 075413 (2017).